Supporting Information

Pumir *et al.* 10.1073/pnas.0711884105

SI Text

Model of Invertebrate Phototransduction: Kinetic Equations. The phototransduction cascade is described by a set of chemical equations. Because of the small number of molecules involved in many of the steps and the consequent importance of molecular "shot" noise, we work with expected number of molecules, rather than concentration (the two are related by the microvillus volume factor, 3×10^{-12} μl). The notation $[X]$ denotes concentration, whereas X denotes the expected number of molecules, and X* will refer to the active state of X. It will also be convenient to define all of the parameters to be either dimensionless or have units of inverse time (i.e., ms^{-1}) as will be appropriate for the rates of activation (generically denoted as κ) or deactivation (generically denoted as γ).

$$\frac{dM^*}{dt} = -\gamma_{Rh^*}(1 + g_{Rh^*}f_n)M^* \quad [1]$$

$$\frac{dG}{dt} = -\kappa_{G^*}G \times M^* + \gamma_{Gi}(G_T - G - G^*) \quad [2]$$

$$\frac{dG^*}{dt} = \kappa_{G^*}G \times M^* - \kappa_{PLC^*}PLC_T \times G^* \quad [3]$$

$$\frac{dPLC^*}{dt} = \kappa_{PLC^*}PLC_T \times G^* - \gamma_{PLC^*}(1 + g_{PLC^*}f_n)PLC^* \quad [4]$$

$$\frac{dA^*}{dt} = \kappa_{A^*}PLC^* - \gamma_{A^*}(1 + g_{A^*}f_n)A^* \quad [5]$$

$$\frac{dB^*}{dt} = \kappa_{B^*}(1 + g_{B^*,f}f_p)(A^*/K_{A^*})^m(B_T - B^*) - \gamma_{B^*}(1 + g_{B^*,n}f_n)B^* \quad [6]$$

$$\frac{d[\mathrm{Ca}]}{dt} = \sigma B^*([\mathrm{Ca}]_{\mathrm{ext}} - [\mathrm{Ca}]) - \gamma_{\mathrm{Ca}}([\mathrm{Ca}] - [\mathrm{Ca}]_0) - (\kappa_{C^*}[\mathrm{Ca}] - \gamma_{C^*}[C^*]) \quad [7]$$

$$\frac{dC^*}{dt} = \kappa_{C^*}\mathrm{Ca} - \gamma_{C^*}\mathrm{C}^* \quad [8]$$

Photon absorption at time $t = 0$ causes a change in conformation of a single rhodopsin molecule into an active metarhodopsin state so that $M^*(0) = 1$. Eq. **1** describes the decay of the expected number, $M^*(t)$, of active metarhodopsin molecules with time. The f_n term on the right-hand-side (defined in Eq. **10**) parameterizes negative feedback, which accelerates M^* inactivation once the inhibitor C^* accumulates. Eqs. **2** and **3** describe activation of G protein by M^*, binding of the active moiety, G^* and PLCβ, which together form an active PLC complex, PLC^*, and the recovery of G from the inactive form G_{inactive}. Inactive G is formed upon deactivation of G*. Introduction of this state is meant to represent the fact that activation of $G_{q\alpha}$ by GDP/GTP nucleotide exchange requires $G_{q\alpha}$ in complex with $G_{\beta\gamma}$, whereas hydrolysis of $G_{q\alpha}$-GTP leaves it in monomeric form which has to rebind to $G_{\beta\gamma}$ before it can be reactivated. The number of inactive G molecules is given by $G_{\mathrm{inactive}} = G_T - G - G^*$, which appears on the right-hand-side of Eq. **2**. PLC^* dynamics is governed by Eq. **4**. The last term in Eq. **4** describes deactivation of PLC^*, which we also assume to be accelerated by C^*. We assume that the number of PLC^* remains small compared with the total PLCβ number PLC_T present in the microvillus. Eq. **5** describes production of the activator A^* by PLC^*. As described in *Model Formulation*, A^* was introduced to subsume the ambiguity of the molecular identity of the activator. The simplest interpretation of this equation would be in terms of the production of DAG from PIP_2 catalyzed by PLC* (with $\kappa_{A^*} \sim [PIP_2]$) and its degradation (through action of DAG-kinase). Eq. **6** describes opening of TRP and TRPL channels, with B^* denoting the open state (the total number is conserved: $B + B^* = B_T$). The precise mechanism of TRP/TRPL activation is not known, but is believed to involve DAG signal. Hence, we assume that transition to B^* state occurs with a rate proportional to $[A^*]^m$ (we shall set $m = 2$, because some cooperativity is necessary to achieve good fits). Eq. **7** describes Ca influx through open TRP* channels and its rapid turnover by the Ca/Na/K exchanger, whose rate is parameterized by γ_{Ca}. Eq. **7** also includes the effect of Ca binding to an abundant protein, C, (such as calmodulin), which acts as a Ca buffer (see additional discussion below). We assume that in its Ca-bound form, C^*, this buffer protein mediates negative feedback. C^* dynamics is described by Eq. **8**. The significant role of Ca buffering is deduced from the fact that, whereas $\gamma_{\mathrm{Ca}}$is estimated to be $\approx$10 ms^{-1} (see *Ca Dynamics*, below), observed Ca decay after light-induced response has a slow tail $\approx$100 ms (1). The latter implies that $\gamma_{C^*} \approx 0.01$ ms^{-1} (provided $\gamma_{\mathrm{Ca}} \gg \kappa_{C^*}$).

In an experiment where a brief, dim flash of light is delivered to the system, activation of one rhodopsin receptor leads to $M^* = 1$. We also assume that in the dark there are no activator ($A^* = 0$), no open channels ($B^* = 0$), internal $[Ca^{2+}] = [Ca^{2+}]_0$, and the number of (Ca-dependent) inhibitor molecules C^* that mediate negative feedback is given by the equilibrium obtained by setting the right-hand side of Eq. **8** to zero.

We have introduced Ca-dependent positive feedback onto the TRP channel opening rate, Eq. **6** via a Hill function $f_p(\mathrm{Ca})$:

$$f_p(\mathrm{Ca}) = \frac{([\mathrm{Ca}]/K_p)^{m_p}}{1 + ([\mathrm{Ca}]/K_p)^{m_p}} \quad [9]$$

Similarly, the negative feedback that is assumed to accelerate deactivation of many of the signaling intermediates (Eqs. **1** and **4-6**) is parameterized by $f_n(C^*)$:

$$f_n(C^*) = \frac{([C^*]/K_n)^{m_n}}{1 + ([C^*]/K_n)^{m_n}} \quad [10]$$

The negative Ca feedback is assumed to act by accelerating the transition of TRP channel from open to refractory states and by accelerating M^* and PLC^* and A^* deactivation. We found that temporal delay in negative feedback introduced by making it depend on the buffered form of Ca, C^*, is essential to adequately describe observed QB waveform. The characteristic [Ca] for the positive feedback is set by K_p. The characteristic $[C^*]$ for the negative feedback is set by K_n. The strength of feedback is parameterized by g_i, which is different for different processes. Lumping all Ca^{2+}-dependent inhibitory processes into a single dynamical variable C^* with a single characteristic K_n and Hill constant m_n is obviously a simplification, but it provides a practical initial approximation for assessing the experimental consistency of model in lieu of more complete mechanistic knowledge about these different processes.

Parameter values used for comparison with the data are collected in Table S1. The equations defined above define a phenomenological model of phototransduction, with many of the parameters corresponding to effective rates that, in principle, depend on the kinetic constants and concentrations of cascade intermediates.

Ca Dynamics. Estimating Ca influx into a microvillus (40% of ≈10-pA current, which translates into $>10^7$ Ca^{2+} ions per second) suggests that internal $[Ca^{2+}]_{in}$ could rapidly rise >1,000-fold, from 0.5 μM, characteristic of the dark state, to the extracellular $[Ca^{2+}]_{ex} \approx 1.5$ mM. This is because, in the tiny, 3×10^{-12} μl, volume of a microvillus, 1 μM corresponds to approximately two molecules and 1.5 mM to 3,000 molecules, which at the rate estimated above would accumulate in a mere 0.3 ms. However, experimental measurements show that transient $[Ca^{2+}]_{in}$ peaks at ≈200 μM and decays with characteristic time scale of 100 ms (2). This implies that Ca influx is counterbalanced with rapid efflux driven by the Ca/Na/K exchanger pumping Ca out with a rate of order 10 ms^{-1}. An additional contribution could be due to rapid uptake of free Ca by Ca-binding proteins, such as calmodulin, which binds Ca with ≈10 μM affinity (3) and is abundant (≈0.5 mM) within microvilli (4). In either way, the time constant of $[Ca^{2+}]_{in}$ is so much faster than any other time constants that it may be considered to be in quasiequilibrium. The observed relatively slow decay of $[Ca^{2+}]_{in}$ after light-induced depolarization is likely to be due to relatively slow release of Ca from its buffer.

Another important consideration concerns the Ca ion exchange between the microvillus and the soma. Ca flux from the microvillus into the soma can be estimated as $DA/L[Ca^{2+}]_{in}$ (where $D \approx 10^3$ $\mu m^2/s$ is Ca^{2+} diffusivity, L is microvillus length, and A is its cross-section area) and comes out to be of order 10^5 ions per second, which is considerably smaller than the influx and efflux currents estimated above. It would nevertheless play a role on longer time scales relevant for light adaptation. We also estimate that on the 1-ms characteristic time of the QB Ca^{2+} ions diffuse over $\sqrt{D\tau} \approx 1$ μm, which means that $[Ca^{2+}]$ can be assumed to be uniform over the volume of the microvillus.

Conversion from the Kinetic to Master Equations. Any kinetic equation has the form

$$\frac{d}{dt}X = R_+(X) - R_-(X), \qquad [11]$$

where X refers to the number of molecules and R_+ and R_- are, respectively, the forward and the reverse reaction rates. The more general probabilistic description is given by the master equation for the probability of having exactly X, Y molecules

$$\frac{d}{dt}p(X,t) = R_+(X-1)p(X-1,t) + R_-(X+1)p(X+1,t) - [R_+(X) + R_-(X)]p(X,t). \qquad [12]$$

This directly generalizes to the case of N molecular species and N reactions in which case X is an array with N components, and the right-hand-side of Eq. **12** sums over N reactions analogous to Eq. **11**.

Stochastic simulation of the master equation derived from Eqs. **1-8** was carried out via the Gillespie algorithm (5) implemented in custom-written Matlab and Fortran programs available upon request from A.P. or B.I.S.

Relating WT QB Properties to Model Parameters. In *Model Formulation*, we have identified the regime of reliable QB generation by the condition that the typical level of A* at the moment of opening the first TRP channel is sufficiently high to cause immediate opening of additional channels leading to a full QB: $A_T > A_{QB}$. Let us make some simple estimates for these quantities.

Ignoring fluctuations, and assuming that the level of PLC* is fixed and that the negative feedback remains small, we find as a solution of Eq. **5**:

$$A^*(t) = \frac{\kappa_A PLC^*}{\gamma_A}(1 - e^{-\gamma_A t}), \qquad [13]$$

which shows that the number of A^* at times shorter than γ_A^{-1}grows approximately linearly, $A^*(t) \approx t\kappa_{A^*}PLC^*$ before saturating at $A^*_{sat} = \gamma^{-1}_{A^*}\kappa_{A^*}PLC^*$. For the WT regime, QB is typically triggered before saturation is reached. The "trigger" level, A^*_T, of the activator can be estimated by requiring that at $A^* = A^*_T$, the rate of channel opening, $\kappa_{B^*}B_T(K^{-1}_{A^*}A^*_T)^m$, becomes equal to the rate of raising A^*, so that $\kappa_{B^*}B_T(K^{-1}_{A^*}A_T)^m = \kappa_{A^*}PLC^*$ and $A^*_T = K_{A^*}(\kappa^{-1}_{B^*}B^{-1}_T\kappa_{A^*}PLC^*)^{1/m}$. This makes explicit the dependence of A^*_T on the level of PLC^*. The latter is determined by the balance of the rates of G^* and PLC^* production (under the assumption of rapid conversion of G^* to PLC^*, i.e., $\kappa_{PLC^*}PLC_T \gg \gamma_{PLC^*}$) with the rate of PLC^* deactivation γ_{PLC^*}:

$$PLC^* = \frac{\kappa_{G^*}G}{\gamma_{PLC^*}}. \qquad [14]$$

Of course, because PLC^* numbers are small, the fluctuations about the average given by Eq. **14** are significant. Note, that A^*_{sat} decreases more rapidly with reduced PLC^* than A_T, which means that at reduced PLC^*, saturation cannot be neglected when estimating A_T. At low PLC^*, A_T saturates at A^*_{sat}.

Condition for QB generation. QB are reliably generated if opening of a single channel entails, with high probability, activation of many more channels. A_{QB} is defined by the condition that a single open channel is not likely to close before the second channel opens.

$$(A_{QB}/K_{A^*})^m = \frac{\gamma_{B^*}}{\kappa_{B^*}(B_T - 1)[1 + g_{B^*,p}f_p([Ca]_{(B^*=1)})]}, \qquad [15]$$

with the positive feedback driven by $[Ca^{2+}]$ set to equilibrium level with one channel open:

$$[Ca]_{(B^*=1)} = \frac{\sigma[Ca]_{ext}}{(\sigma + \gamma_{Ca} + \kappa_{C^*})} \qquad [16]$$

Eqs. **15** and **16** provide an explicit expression for A_{QB} ($[Ca^{2+}]_{ex}$). Because at low PLC^* $A^*_T = A^*_{sat}$, the minimal PLC^* threshold for QB generation is given by $A^*_{sat}(PLC^*) = A_{QB}([Ca^{2+}]_{ex})$ condition.

An important characteristic of a QB is the decoupling of the time-scales of A^* growth and B^* opening, once the first channel opens. Acceleration of B^* opening is due to the positive feedback provided $g_{B^*,p}f_p([Ca]_{(B^*=1)}) > 1$, which defines the minimal $[Ca^{2+}]_{ex}$ boundary of the QB domain in Fig. 2*c*. (This assumption that the Ca pump rate is faster than the buffering rate is not essential and is made only for the sake of simplicity.) For $[Ca^{2+}]_{ex}$ below that level, B^* activity follows A^* level adiabatically. We shall return to effect of positive feedback in *Role of DAG Kinase and the Molecular Nature of A**, below.

Estimating QB Latency. A more rigorous probabilistic description of the QB "triggering" is obtained via the "first passage" type analysis (6), which in general determines the probability of a given event to occur for the first time during a given time period.

The probability of opening the first channel during the time interval $(t, t + dt)$ based on Eq.**6** (with $B^* = 0$) is given by

$$P_+(t)dt = \exp\left[-\int_0^t dt'\,\kappa_B B_T [K_A^{-1} A^*(t')]^m\right] \kappa_B B_T [K_A^{-1} A^*(t)]^m dt. \quad [17]$$

A_T^* crudely estimated above can be determined by substituting $A^*(t)$ in the linear regime and maximize $P_+(t)$w.r.t. t which defines t_T and $A_T^* = A^*(t_T)$.

The average time before the first channel opens is

$$\int_0^\infty dt\, tP_+(t)dt,$$

which in the linear $A^*(t)$ regime gives the following estimate for the mean latency time:

$$\langle t_L \rangle \approx (m+1)^{1/(m+1)} \Gamma\left(\frac{m+2}{m+1}\right) \left[\frac{K_A^m}{\kappa_B B_T \kappa_A^m P L C^{*m}}\right]^{1/(m+1)}, \quad [18]$$

where Γ is the Euler Gamma function, and the m-dependent prefactor is a number of order 1.

From Eqs. **14** and **18**, we see that decreasing the total number of G proteins or decreasing the total number of TRP channels (B_T) should cause increased QB latency with the latter having a weaker effect.

Note that the above analysis is not limited to $A^*(t) \approx t$ regime and can readily be extended to include saturation effects and A^* fluctuations.

Estimating QB amplitude. We will now show that increasing A_T translates into a higher QB amplitude. Peak B^* value, $B^*_{\max}$, is determined by the condition that the rates of opening and closing the channel should be equal:

$$\kappa_{B^*}(1 + g_{B^*,p} f_p(\mathrm{Ca}))(A_T/K_{A^*})^m (B_T - B^*) = \gamma_{B^*}(1 + g_{B^*,n} f_n(C^*))B^* \quad [19]$$

so that

$$B^*{}_{\max} = \frac{(A_T/K_{A^*})^m B_T}{(A_T/K_{A^*})^m + \dfrac{\gamma_{B^*}[1 + g_{B^*,n} f_n(C^*{}_B)]}{\kappa_{B^*}[1 + g_{B^*,p} f_p(\mathrm{Ca}_{\max})]}} \approx \frac{(A_T/K_{A^*})^m B_T}{(A_T/K_{A^*})^m + \dfrac{\gamma_{B^*}[1 + g_{B^*,n}(C_B^*/K_n)^{m_n}]}{\kappa_{B^*}(1 + g_{B^*,p})}}, \quad [20]$$

which shows a sigmodial dependence on A_T. Eq. **20**, however, must be supplemented by expressions for $\mathrm{Ca}_{\max}$and $C_B{}^*$. Because Ca dynamics is very fast, peak $\mathrm{Ca}_{\max}$ is related to peak B^* approximately by $[\mathrm{Ca}_{\max}] = \sigma\,[\mathrm{Ca}]_{\mathrm{ex}} B^*_{\max}/\gamma_{\mathrm{Ca}}$, which for WT $[\mathrm{Ca}]_{\mathrm{ex}}$, and our parameters drops out of Eq. **20** (second line) because of saturation of the positive feedback $[\mathrm{Ca}_{\max}] \gg K_p$.

The level of the inhibitor setting QB peak, C_B^*, is determined dynamically:

$$[C_B^*] = \kappa_{C^*} \int_0^{t_B} dt' e^{-\gamma_{C^*}(t-t')} [\mathrm{Ca}(t')] \approx \frac{\kappa_{C^*} \gamma_{\mathrm{Ca}}^{-1} \sigma [\mathrm{Ca}]_{\mathrm{ex}} (B^*_{\max})^2}{2\kappa_{B^*}(1 + g_p) B_T (A_T/K_{A^*})^m}, \quad [21]$$

the last line derived under the assumption that the characteristic time of C^* decay, $1/\gamma_{C^*}$is much longer than the "time to peak"

$$t_{\mathrm{peak}} \approx \frac{B^*{}_{\max}}{\kappa_{B^*}(1 + g_p) B_T (A_T/K_{A^*})^m}. \quad [22]$$

Finally, $B^*_{\max}$ and $[C_B^*$ are determined self-consistently by solving Eqs. **20** and **22** together, which yields the dependence of QB amplitude on $[\mathrm{Ca}]_{\mathrm{ex}}$ and on A_T and hence PLC^* and G.

When Does the Positive Feedback Turn On? As illustrated in Fig. 2*a*, generation of QBs under physiological conditions ($[\mathrm{Ca}^{2+}]_{\mathrm{ex}}$ = 1.5 mM) occurs via an integrate-and-fire process: The number of activator molecules, A^*, grows, until a TRP-channel opens (B^* jumps to 1), with more channels rapidly opening thereafter driven by positive feedback. This is to be contrasted with the situation at very low $[\mathrm{Ca}^{2+}]_{\mathrm{ex}}$, where the opening of a limited number of channels is a slow process. Our model allows us to quantitatively analyze the generation of QB, and to determine a threshold in the external Ca concentration above which the response is a nonlinear process, leading to genuine QB. Investigating the transition between the two response regimes helps to understand the features of the Ca^{2+}-dependence of the QB response, shown in Fig. 5.

To analyze the opening of TRP-channels, we consider here only the B module, see Fig. 1, and study the response as a function of the input: the number of activator molecules, A^*, and as a function of $[\mathrm{Ca}^{2+}]_{\mathrm{ex}}$. The amount of inhibitor C^* during the early stage of QB generation is small, so the negative feedback can be neglected: $f_n = 0$. The analysis of the dynamics of TRP-channel opening, is carried out by first determining, the fixed points (i.e., possible equilibria) of B^* as a function of A^* and $[\mathrm{Ca}^{2+}]_{\mathrm{ex}}$. Because of the fast equilibration of the intracellular Ca concentration allows us to set $[\mathrm{Ca}^{2+}]_{\mathrm{in}}$ to its equilibrium value from Eq. **7**: $[\mathrm{Ca}^{2+}] \approx [\mathrm{Ca}^{2+}]_{\mathrm{ex}}\ \sigma B^*/\gamma_{\mathrm{Ca}}$ and to compute the positive feedback computed with this value, which leads to the cubic equation for the fixed points of B^* ($dB^*/dt = 0$ in Eq. **6**):

$$B^{*3} \frac{\sigma^2 [\mathrm{Ca}]_{\mathrm{ext}}^2}{\gamma_{\mathrm{Ca}}^2} (\kappa_{B^*}(1 + g_{Bp}) \times (A^*/K_A)^m + \gamma_{B^*}) - B^{*2} B_T \frac{\sigma^2 [\mathrm{Ca}]_{\mathrm{ext}}^2}{\gamma_{\mathrm{Ca}}^2} \kappa_{B^*}(1 + g_{Bp}) \times (A^*/K_A)^m + B^*(\kappa_{B^*} K_p^2 \times (A^*/K_A)^m + \gamma_{B^*}) - (\kappa_{B^*} K_p^2 \times (A^*/K_A)^m + \gamma_{B^*}) B_T = 0. \quad [23]$$

The number of real solutions of the cubic equation for $\mathbf{B}^*$, Eq **23**. can be 1 or 3 depending on A^* and $[\mathrm{Ca}^{2+}]_{\mathrm{ex}}$. At very low or high levels of $[\mathrm{Ca}^{2+}]_{\mathrm{ex}}$, there is only one root and hence only one B^* fixed point. However, in the region of parameter space limited by the black dashed lines in Fig. S1, Eq. **23** has three roots and hence three B^* fixed points. This is the region of bistability: for a range of values of A^*, the system has two stable fixed points corresponding to one low and one high value of B^* and one unstable fixed point at an intermediate value of B^*. A very fast transition occurs then when B* is larger than the intermediate, unstable fixed point. This type of analysis is usually done in the continuum limit, but in our case, B^* is a number of open channel, not concentration, and therefore can only take integer values.

Thus a fixed point at $B^* < 1$ is unphysical. Hence, we look for a line in parameter space where $B^* = 1$ is a fixed point of Eq. **20**, indicated in Fig. S1 by the blue-red line. At high values of $[Ca^{2+}]_{ex}$ (red line), $B^* = 1$ is unstable. This implies that once a single TRP channel is open, more channels will rapidly open, thus leading to a QB. On the other hand, at lower values of $[Ca^{2+}]_{ex}$ (blue line), $B^* = 1$ is a stable solution. In this case, opening one channel is not enough to start a QB. However, for $[Ca^{2+}]_{ex}$ above $\approx 80\ \mu$M, B module still has a bistable regime and is capable of excitable media response: Fluctuation-induced opening of one or more additional channels can still induce a "regenerative spike" of channel opening, also known as a QB. For $[Ca^{2+}]_{ex}$ below $\approx 80\ \mu$M, the nonlinearity never really sets in, and QB cannot be generated. In this regime, B^* (close to its fixed point value) follows the dynamics of A^* (assumed to be slower than the dynamics within the B module) and therefore generates a relatively slow "adiabatic" response.

The nature of the cross-over can be conveniently illustrated by computing the histograms of QB amplitudes, B^*_{max}, see Fig. S2. At low $[Ca^{2+}]_{ex}$ concentration, the distribution peaks at approximately five to six open channels. When $[Ca^{2+}]_{ex}$ gets close to the QB generation "threshold" $[Ca^{2+}]_{ex} \approx 80\ \mu$M, a second peak B_{max} close to saturation appears and becomes the dominant one at $[Ca^{2+}]_{ex} = 150\ \mu$M. As $[Ca^{2+}]_{ex}$ increases toward the physiological value the lower peak of B_{max} distribution disappears and the upper peak shifts to somewhat lower values because of the negative feedback. The peak in the coefficient of variation of the response amplitude seen in Fig. 5 is due to the bimodality of the response in the transition region, where only a fraction of events result in a QB.

The Role of DAG Kinase and the Molecular Nature of *A.** Can we understand the reported effect of reduction of DAG kinase (DK) or *norpA* activity (7), which leads to a larger QB amplitude? We have two possible interpretations for DAG kinase activity. In *Case a*, A^* is identified with DAG so that A^* degradation rate γ_{A*} is proportional to DAG kinase activity. In *Case b*, A^* is identified with DAG a product such as PUFA (8) downstream of DAG.

Case a. Explaining low *dgq* yield has lead us to the regime $\gamma_{PLC*} \gg \gamma_{A*}$,where $\gamma_{A*}$and hence DAG kinase has only a weak effect on QB initiation. However if the C^*-activated destabilization of A^* depended on DAG kinase activity (as in our Eq. **5**), reduction of γ_{A*}relative to the WT would increase QB amplitude (see our estimate of QB amplitude in *Estimating QB Amplitude*) although the effect would be rather weak.

Case b. Suppose A^* is produced from DAG (e.g., PUFA) via

$$\frac{d}{dt}A^* = \kappa_{PUFA}DAG - \gamma_{PUFA}A^*, \qquad [24]$$

whereas DAG is established by the balance of the PLC^*, and DAG kinase activities the latter setting the degradation rate γ_{DAG}

$$\frac{d}{dt}DAG = \kappa_{DAG}PLC^* - \gamma_{DAG}DAG. \qquad [25]$$

If we assume that DAG equilibrates relatively rapidly so that so that

$$DAG = \frac{\kappa_{DAG}}{\gamma_{DAG}}PLC^* = \frac{k_{DAG}[PIP_2]}{k_{DK}[DK]}PLC^* \qquad [26]$$

(where DK refers to DAG kinase) so that the effective parameters of our module A (Eq. **5**) are identified as $\gamma_{A*} = \gamma_{PUFA}$ and

$$\kappa_{A^*} = \frac{k_{DAG}[PIP_2]}{k_{DK}[DK]}\kappa_{PUFA}. \qquad [27]$$

This tells us that the reduction of DAG kinase activity, just like an increase in $[PIP_2]$, has the effect of increasing κ_{A*},which in turn has the effect of increasing the QB yield (by increasing Y_A) and increasing QB amplitude by increasing A_T.

Our comparison of Case *a* and Case *b* scenarios suggest that Case *b* with PUFA acting as A^* is more likely to account for the strong observed effect of ATP deprivation (9), which reduces DAG kinase activity. The two cases according to our analysis can be distiguished by looking at the QB yield of the *dgq* mutant: In Case *a* it is not affected by reduction of DAG kinase activity; in Case *b*, it is increased.

Dependence on External Ca^{2+} Concentration. The external Ca concentration can be readily varied in an experiment, as was done by Henderson *et al.* (10), who measured the mean QB amplitude and the corresponding coefficient of variance (i.e., the ratio between the root mean square variation and the mean) as well as the mean latency time for different $[Ca^{2+}]_{ex}$.

The predictions of the model are shown in Fig. 5. The model predicts that at low Ca^{2+}, the amplitude remains essentially constant and small, but as the external Ca^{2+} concentration $[Ca^{2+}]_{ex}$ increases beyond a certain threshold, the average amplitude goes up. This corresponds to the point where positive Ca^{2+} feedback becomes important. The coefficient of variation (c.v.) peaks at the cross-over from the low to high amplitude response, the latter corresponding to the QB regime. This peak is explained in *When Does the Positive Feedback Turn On?*, above, and is due to the bimodality of the predicted response in the cross-over regime. Average amplitude peaks at $[Ca^{2+}]_{ex}$ level when the negative feedback becomes important. At higher $[Ca^{2+}]_{ex}$, average QB amplitude diminishes because of the effect of strong negative feedback. The latency time is predicted to decrease slightly as $[Ca^{2+}]_{ex}$ increases.

At very low external Ca^{2+} concentration $[Ca^{2+}]_{ex} < 0.01$ mM, response passively follows the level of PLCβ activity, as indicated by the long value of the half-width. Positive Ca^{2+} feedback becomes important for $[Ca^{2+}]_{ex} \approx 0.02$ mM, resulting in regenerative opening of an increased number of channels over a shorter time—the QB events. The peak in the coefficient of variation occurs at the cross-over between the passive and regenerative response, because of response bimodality in that regime (see *Dependence on External Ca^{2+} Concentration*). At $[Ca^{2+}]_{ex} > 0.5$ mM, the negative feedback becomes important, reducing the peak number of open channels. The trends shown in Fig. S2 are generally consistent with the results of ref. 10, including, in particular, the peak in the coefficient of variation of the QB amplitude. On the other hand, the dependence of the latency time on $[Ca^{2+}]_{ex}$ predicted by the model appears to be too weak, suggesting that the model has omitted the Ca^{2+} dependence for some of the processes involved in module A.

Numerical Determination of the Model Parameters. The parameters of the model shown in the table below were determined by fitting the properties of the QBs, obtained experimentally from a set of 83 records, with the model results, determined from a large number of simulated QBs (typically 40,000). The parameters of the model were systematically varied to satisfy a number of constraints, which are imposed via the cost function, defined in turn.

(1) The mean experimental value of the time to the peak value of the QB was $t_{peak,exp} = 87$ ms, whereas the time from half-peak amplitude to peak amplitude, denoted by t_2 in (10) is found to be $t_{2,exp} = 8.4$ ms, and the time from peak amplitude to half-amplitude, denoted t_3, is $t_{3,exp} = 11.2$ ms. The sum $t_{1/2} = (t_2$

$+ t_3$) characterizes the width of the QB. To impose that the ratio of time scales predicted by the model $t_{peak,mod}$ and that $t_{1/2,mod}$ be the same as the experimental one, we introduce the term in the cost function:

$$C_{Time} = 1{,}000 \times (t_{1/2,mod}/t_{peak,mod} - t_{1/2,exp}/t_{peak,exp})^2. \quad [28]$$

(2) Averaging the experimental pulse shapes by aligning QB according to the method described in ref. 10 allowed us to determine an experimental mean shape, $B_{mean,exp}$. This shape differs significantly from 0 over a time range on the order of 30 ms around the peak amplitude. To keep the difference between the experimental shape and the model-predicted shape $B_{mean,mod}$ small, we introduced the cost function:

$$C_{Shape} = 100 \times \frac{1}{(t_+ - t_-)} \int_{t_-}^{t_+} (B_{mean,exp}(t') - B_{mean,mod}(t'))^2. \quad [29]$$

(3) The coefficient of variability of the amplitude, cv_{amp}, defined as the ratio between the rms and the mean of the QB, was found to be experimentally on the order of $cv_{amp,exp} \approx 0.4$, close to the values found by ref. 10. To maintain the same variability for the solution of the model, $cv_{amp,mod}$, we added a cost function: $C_{cv,amp} = 5 \times (cv_{amp,exp} - cv_{amp,mod})^2$.

(4) The number of *PLC** molecules involved during the generation of a QB is on the order of 5 (11). Taking into account Eq. **15** above, we introduced the following cost term:

$$C_{PLC^*} = 2 \times \ln\left(0.2 \times \frac{G_t \kappa_G}{\gamma_{PLC^*}}\right)^2 \quad [30]$$

(5) The response at very low external Ca^{2+} concentration is smaller than at physiological Ca^{2+} concentration. In the absence of any feedback ($[Ca]_{ext} = 0$), the number of open TRP channels is determined by the quantity: $\zeta = \kappa_{B*}(B_T \kappa_{A*} \kappa_{G*} G_T / \gamma_{PLC*} \gamma_{A*} K_T)^3 / \gamma_{B*}$. The response at low Ca^{2+} concentration is made small by adding the following cost term: $C_{Ca=0} = 4 \times \ln(9 \times \zeta)^2$.

The total cost function is obtained by summing up the five contributions above. The precise numerical value of the coefficients is somewhat arbitrary; they were adjusted empirically to ensure that the solution matches very well the experimental profiles and the time scale ratio t_2/t_{peak}.

The parameter search is reduced to a minimization of this cost function. This can be done by hand, or by using the simplex algorithm "amoeba" described in "Numerical Recipes."

With the program written in Fortran, the computation of a set of 40,000 QBs takes ≈1 mn of CPU on a PC.

Parameter Sensitivity Analysis. The model has many unknown parameters. Our analysis above has attempted to identify combinations of parameters that control various features of the QB: e.g., latency, amplitude, etc. However, we could not analytically reduce the model to the "minimal" form explicitely identifying the complete set of "effective" parameters (themselves being combinations of explicit parameters of the model) controlling the response. On the other hand, the process of data fitting revealed that an excellent fit is achievable on a manifold of parameters, suggesting redundancy, which we understand in terms of "lumping" of parameters into a smaller number of combinations that control the response. Of course, the issue of parameter sensitivity is central to modeling in systems biology and has been investigated in other contexts. Brown, *et al.* (12) in particular noted the existence of exponentially "soft" (i.e., insensitive) directions in the parameter space.

To quantitatively assess parameter sensitivity, we investigated local variation of the cost function as a function of the parameters. This cost function C is the sum of the five terms listed in *Numerical Determination of the Model Parameters*, above, involving the difference between experimentally measured quantities and model predictions. Its dependence on the following 18 parameters: ($K_p, K_m, K_T, \kappa_{A*}, \kappa_{PLC*}, \kappa_{G*}, \kappa_{C*}, \gamma_{B*}, \gamma_{A*}, \gamma_{C*}, \gamma_{PLC*}, \gamma_{G*}, \gamma_{Ca}, g_{Bp}, g_{Bm}, g_{Am}, g_{PLC*}, \sigma$), denoted generically α, is studied by varying $C(\alpha)$ near the minimum C_{min}, obtained for a set of values α_{min}. The first derivatives of C with respect to the parameters α are all zero at α_{min}. The dependence of the solution on the parameters is characterized, close to the equilibrium, by the Hessian matrix of C:

$$H_{ij} = \left(\frac{\delta^2 C}{\delta \ln(\alpha_i)\, \delta \ln(\alpha_j)}\right)_{\alpha = \alpha_{min}} \quad [31]$$

The Hessian H is a real, symmetric, 18^2 matrix. Because the problem studied here is intrinsically stochastic, the values $C(\alpha)$ computed numerically with a large, albeit finite, number of realizations N_r are contaminated by noise. On general grounds, it is expected that the aamplitude of the noise is of the order of $\varepsilon \propto 1/\sqrt{N_r}$. The values of $C(\alpha)$ can therefore be written as: $C(\alpha) = C_0(\alpha) + \varepsilon\chi$, where χ is a noise term of order 1, essentially uncorrelated between different values of α ("white"). As a result, the computed value of the Hessian H is expected to be of the order of $H(\alpha) = H_0(\alpha) + (\varepsilon/(\delta\ln(\alpha))^2)\eta$, where η is the noise term, *a priori* of order 1. Therefore, to control the noise, one has to make sure that $\varepsilon/(\delta\ln(\alpha))^2$ is small enough. With the number of realizations chosen for most of the calculations here, N_r = 40,000, the value of ε is of the order of $\varepsilon \approx 5.10^{-3}$. The calculation was also run for N_r = 160,000. Eigenvalue spectra obtained with different step sizes (for $\delta\ln(\alpha)$ = 0.2, 0.4, 0.6, and 0.8), and N_rs are shown in Fig. S3. The results show that the spectrum is dominated by noise at small values of $\delta\ln(\alpha)$ (0.2 and 0.4), but appears to have converged for two of the largest values: $\delta\ln(\alpha) = 0.6$ and 0.8. The convergence is particularly clear for the top five eigenvalues, which account for >90% of the variation. The corresponding eigenvectors have a well defined structure in the parameter space. The distribution of smaller eigenvalues plausibly converges toward an exponential at large values of the index, similar to the results found in ref. 12. However, in contrast to the largest modes, the structure of the corresponding eigenvectors is not well defined. The matrix H is also found to have of this a few small negative eigenvalues, which we interpret as very small eigenvalues of $H_0(\alpha)$ turned negative due to the effect of the noise.

In summary, the above analysis confirms that our fit is quite robust with only five parameter combinations being critically constrained by the fit. However, we believe that this does not reflect full redundancy of parameters and expect that an attempt to fit additional experimentally measured quantities will increase the number of constraints.

Details of the Whole-Cell Recording Method. Retinas from newly eclosed flies were prepared as previously described (13, 14). The cells were allowed to gently settle under bath solution (see below) onto a glass coverslip forming the bottom of the recording chamber and were visualized through Hoffman interference contrast on a Zeiss Axiovert 135 inverted microscope. Whole-cell voltage-clamp recordings were made by using glass electrodes fire polished to a final tip resistance of ≈7 mΩ. Junction potentials were nulled just before seal formation, and cells were held at -50 mV for all recordings. Series resistances were 25 MΩ or below and were typically compensated to >80% for macro-

scopic responses and were uncompensated for QB recordings. Signals were collected by using an Axopatch 200B amplifier (Axon Instruments), low-pass filtered at 500 Hz through an eight-pole Bessel Filter (LPF-8; Warner Instruments) and digitized at 100 kHz by using a PCI-6052E board (National Instruments) for analysis. Acquisition and analysis software was homewritten by using VB.NET (Microsoft). Cells were stimulated by 3-nsec pulses of 480-nm light from a dye module pumped by a VSL-337ND-S nitrogen laser. Laser output was quantitated by using a single-channel joulemeter (EM500; Molectron) and attenuated by neutral density filters (Oriel). The bath solution contained 120 mM $NaCl_2$, 5 mM KCl_2, 10 mM Hepes, 4 mM $MgCl_2$, 24 mM proline, 5 mM alanine, and 1 mM $CaCl_2$ at pH 7.1, and the electrode solution consisted of 140 mM potassium gluconate, 10 mM Hepes, 2 mM $MgSO_4$, 1 mM NAD, 4 mM MgATP, 0.5 mM NaGTP, and 0.5 mM EGTA at pH 7.1. All chemicals were obtained from Sigma.

1. Oberwinkler J, Stavenga DG (2000) Calcium transients in the rhabdomeres of dark- and light-adapted fly photoreceptor cells. *J Neurosci* 20:1701–1709.
2. Postma M, *et al.* (1999) Does Ca^{2+} reach millimolar concentrations after single photon absorption in *Drosophila* photoreceptor microvilli? *Biophys J* 77:1811–1823.
3. Maune JF, *et al.* (1992) Ca^{2+} binding and conformational change in two series of point mutations to the individual Ca(2+)-binding sites of calmodulin. *J Biol Chem* 267:5286–5295.
4. Porter JA, *et al.* (1995) Calmodulin binding to *Drosophila* NinaC required for termination of phototransduction. *EMBO J* 14:4450–4459.
5. Gillespie DT (1976) General method for numerically simulating stochastic time evolution ofof coupled chemical reactions. *J Comp Phys* 22:403–434.
6. Redner S (2001) *A Guide to First-Passage Processes* (Cambridge Univ Press, Cambridge, UK).
7. Hardie RC, *et al*. (2001) Calcium influx via TRP channels is required to maintain PIP2 levels in Drosophila photoreceptors. *Neuron* 30:149–159.
8. Hardie RC (2003) TRP channels in Drosophila photoreceptors: the lipid connection. *Cell Calcium* 33:385–393.
9. Hardie RC (2001) Phototransduction in Drosophila melanogaster. *J Exp Biol* 204:2403–2409
10. Henderson SR, *et al.* (2000) Single photon responses in Drosophila photoreceptors and their regulation by Ca2+. *J Physiol* 524:179–194.
11. Hardy RC, *et al.* (2002) Molecular basis of amplification in Drosophila phototransduction: Roles of G-protein, phospholipase C and diacylglycerol kinase. *Neuron* 14:689–701.
12. Brown KS, *et al.* (2004) The statistical mechanics of complex signaling networks: nerve growth factor signaling. *Phys Biol* 1:184–195.
13. Ranganathan R, *et al*. (1991) The molecular genetics of invertebrate phototransduction. *Trends Neurosci* 14:486–493.
14. Ranganathan R and Stevens C (1995) Arrestin binding determines the rate of inactivation of the G-protein-coupled receptor rhodopsin in vivo. *Cell* 81:841–848.

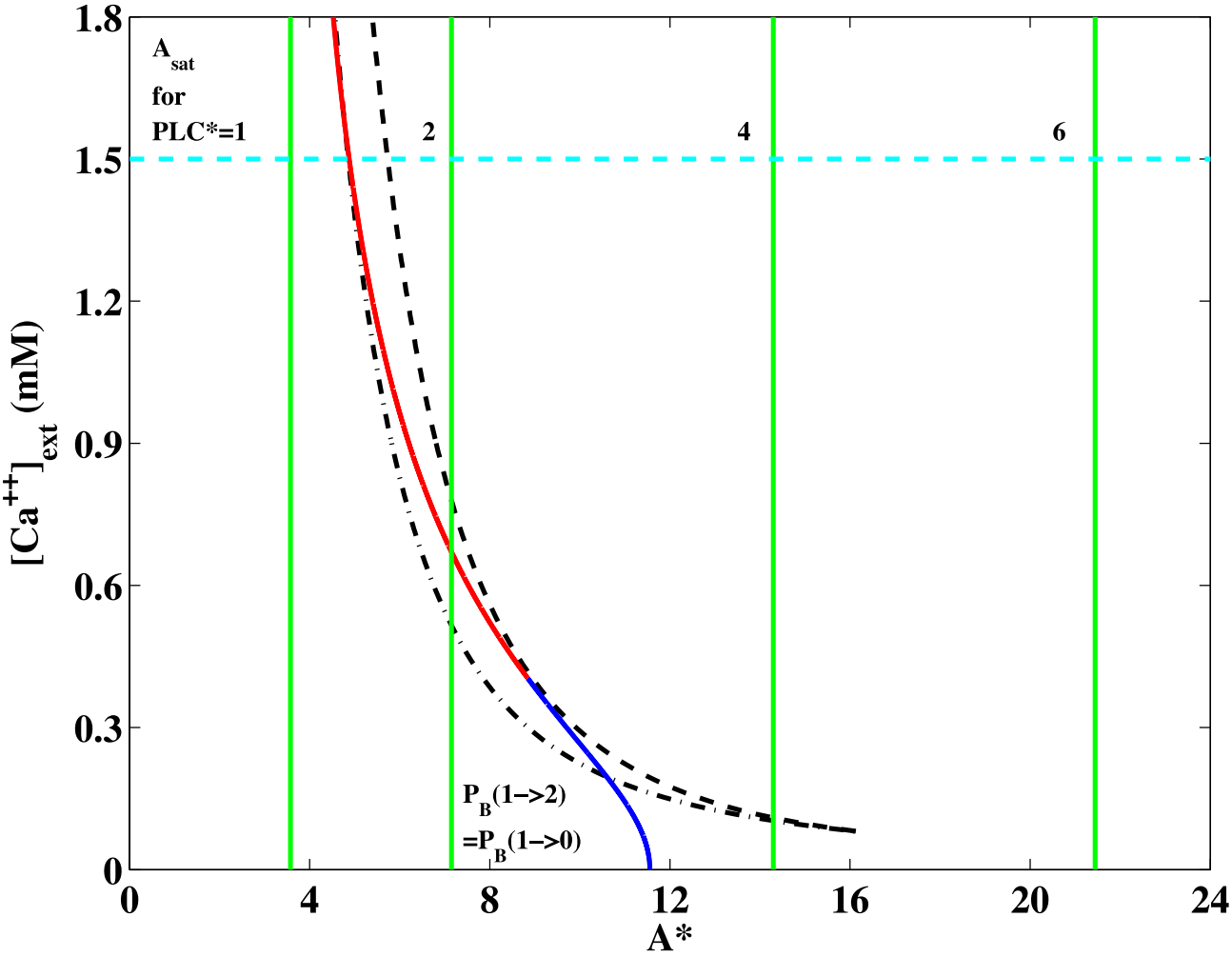

Fig. S1. The (A^*, $[Ca^{2+}]_{ex}$) parameter map of the B module response. The parameters region between the two dashed black lines is the region of bistability in the continuum solution of Eqs. **6** and **23**. The lines in blue-red indicates the location in the (A^*, $[Ca^{2+}]_{ex}$) plane of $B^* = 1$ fixed point: $B^* = 1$ is unstable for $[Ca^{2+}]_{ex}$ large enough (red curve), and stable for low values of $[Ca^{2+}]_{ex}$ (blue curve). The values of A^* obtained for a given level of PLC^* (indicated on the curves) is shown (vertical green curves). The dashed cyan line corresponds to the physiological $[Ca^{2+}]_{ex}$ concentration.

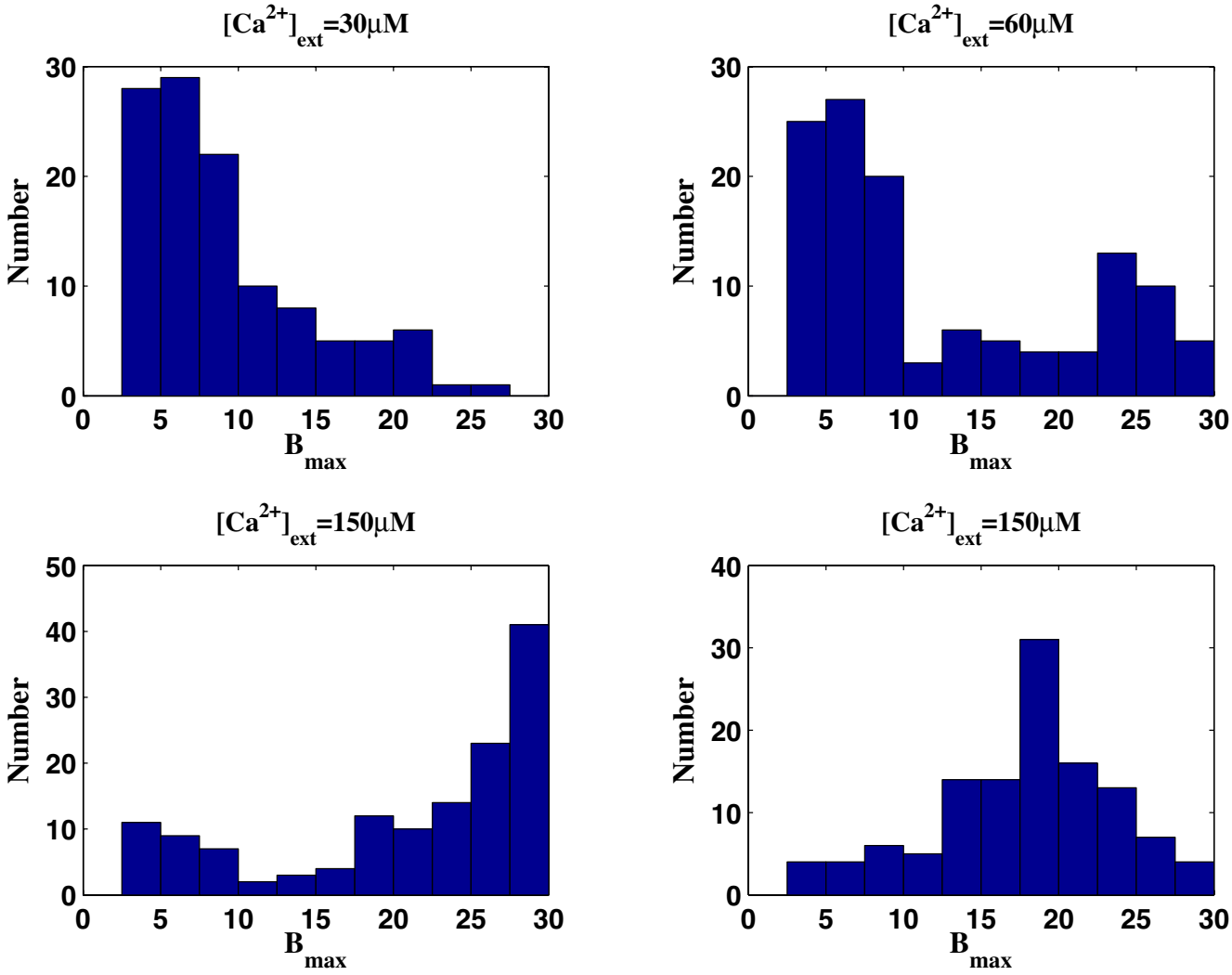

Fig. S2. The probability distribution function of response amplitude, defined as the maximal value of the number of open TRP channels, B_{max} at several values of $[Ca^{2+}]_{ex}$. Two peaks can be observed as for $[Ca^{2+}]_{ex}$, in the cross-over region.

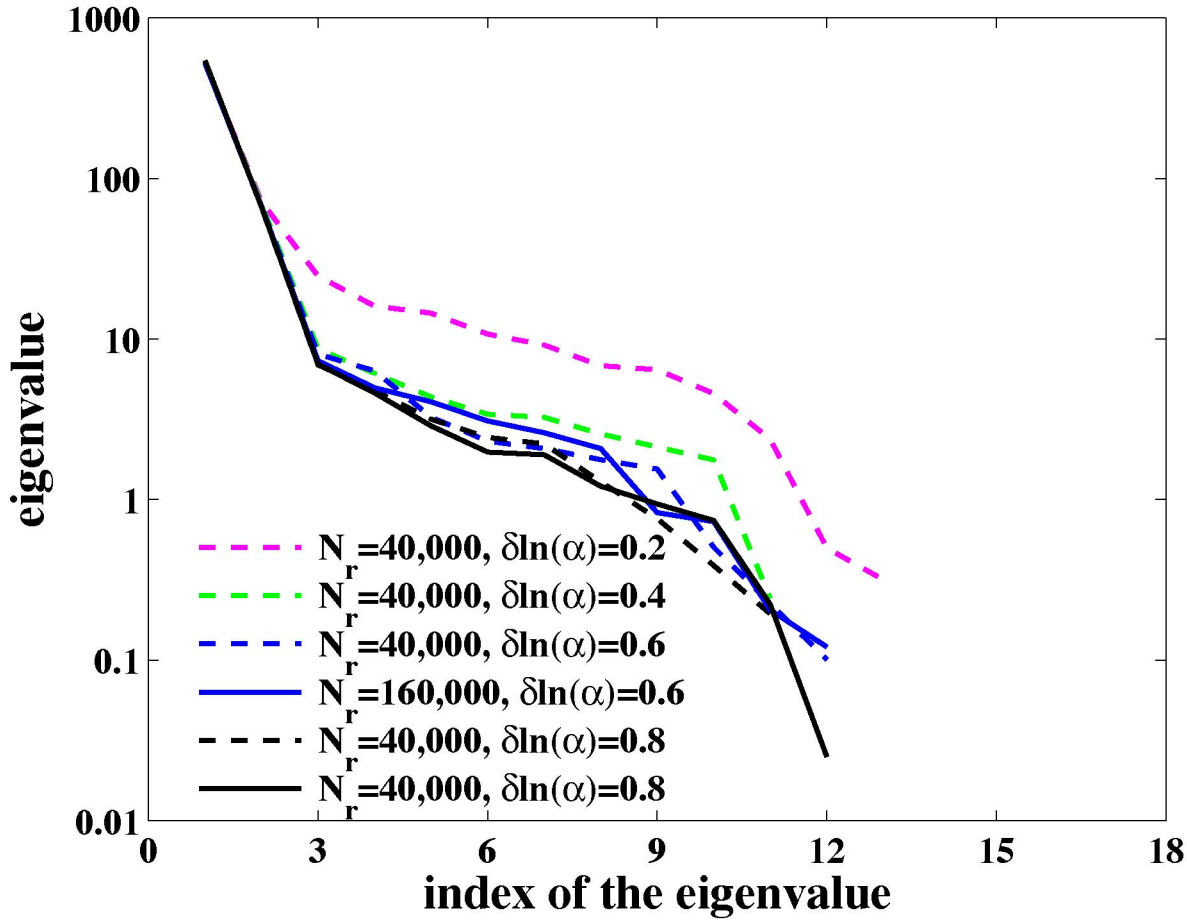

Fig. S3. Spectrum of the Hessian matrix for $\delta\ln(\alpha) = 0.2$, 0.4, 0.6, and 0.8. The spectrum is contaminated by noise for the smallest values ($\delta\ln(\alpha) = 0.2$ and 0.4, whereas the five largest eigenvalues have converged for the largest value of $\delta\ln(\alpha)$.

Table S1. Summary of model parameters

$K_p = 6.2$	K_D for positive Ca feedback (μM)
$K_n = 19.5$	K_D for negative Ca feedback (μM)
$m_p = 2$	Hill constant for positive Ca feedback
$m_n = 3$	Hill constant for negative Ca feedback
$g_{B,p} = 41.5$	Strength of positive Ca feedback on Trp
$g_{B,n} = 5.4$	Strength of negative Ca feedback on Trp
$g_{PLC*} = 11.1$	Strength of negative Ca feedback on PLCβ
$g_A = 37.8$	Strength of negative Ca feedback on A*
$g_{M*} = 8 \times 10^3$	Strength of negative Ca feedback on Rh*
$\kappa_{G*} = 4.7 \times 10^{-3}$	Rate of G* activation (ms^{-1})
$\kappa_{PLC*} = 3.9 \times 10^{-3}$	Rate of PLC activation (ms^{-1})
$\kappa_{A*} = 7.4 \times 10^{-2}$	Rate of sctivator (A*) production (ms^{-1}) expected to be proportional to [PIP_2]
$\kappa_{B*}/K_T^3 = 1.3 \times 10^{-6}$	Rate of TRP (B*) activation (ms^{-1})
$\kappa_{C*} = 1.0 * 10^{-2}$	Rate of C* activation (ms^{-1}) expected to be proportional to [CaM]
$\gamma_{Rh*} = 3.7 \times 10^{-3}$	Deactivation rate of Rh* (ms^{-1})
$\gamma_{Gi} = 3.5 \times 10^{-2}$	Deactivation rate of G* (ms^{-1})
$\gamma_{PLC*} = 4.8 * 10^{-2}$	Deactivation rate of PLC* (ms^{-1})
$\gamma_{A*} = 2.1 * 10^{-2}$	Deactivation rate of activator (A*) (ms^{-1})
$\gamma_{B*} = 6.0 \times 10^{-2}$	Deactivation rate of TRP/TRPL channels (B*) (ms^{-1})
$\gamma_{Ca} = 33$	Rate with which Ca is pumped out (ms^{-1})
$\gamma_{C*} = 5.5 \times 10^{-3}$	Deactivation rate of C* (ms^{-1}).
$\sigma = 0.17$	Influx of Ca ions per TRP/TRPL channel (ms^{-1})
$B_T = 30$	Total no. of TRP/TRPL channels per microvillus
$G_T = 50$	Total no. of G proteins
$PLC_T = 100$	Total no. of PLC molecules